# Comparison of the Corrosion Behavior of TiNi Alloys with Martensitic and Austenitic Structures

*Anna* Churakova[1, 2 *] and *Elina* Kayumova[2, 3]

[1]Institute of Molecule and Crystal Physics - Subdivision of the Ufa Federal Research Center of the Russian Academy of Sciences, 151 pr. Oktyabrya, Ufa, 450075, Russia
[2]Ufa State Aviation Technical University, 12 K. Marx str., Ufa, 450008, Russia
[3] Ufa State Petroleum Technological University, 1 Kosmonavtov st., Ufa, 450064, Russia

**Abstract.** The work is devoted to the study of the corrosion behavior of TiNi alloys with the original austenitic and martensitic structure in various states. In the course of the research, it was found that the rate of corrosion destruction for coarse-grained and ultrafine-grained $Ti_{49.0}Ni_{51.0}$ alloys is different: the coarse-grained alloy turned out to be less corrosion resistant and the destruction rate was higher than the corrosion rate in the ultrafine-grained state. X-ray phase analysis of TiNi alloys revealed that as a result of corrosion processes, a change in the phase composition of the alloy occurs, accompanied by the formation of TiNi hydride - $TiNiH_{1.4}$. In the ultrafine-grained state, the volume fraction of the formed hydride is higher than in the coarse-grained state. This is typical for both alloys, however, in the martensitic alloy, the volume fraction is higher than in the austenitic one.

## Introduction

Martensitic transformations, including in alloys of the TiNi system, occur with a change in the volume of the participating phases [1–2]. Although these changes are minimal, they, as well as other features of the transformations, lead to increased stresses in the interface region - at the boundaries of the transforming phases, which leads to the formation of irreversible crystallographic defects (for example, dislocations in the austenite phase) [2]. The accumulation of such defects leads to a change in the transformation temperatures, the formation of residual martensite, an increase in residual plastic deformations during mechanocycling, etc. [2]. Characteristics of structural and functional fatigue, i.e. maintaining the integrity of the material under cyclic loads and the stability of their functional properties determine the possibility of using the product with a large number of transformation cycles [2-11]. Large effect sizes, the ability to control the transformation temperatures by partially replacing Ni or Ti with other elements (such as Cu, Pd, Pt, Co, Fe, Hf, Nb), good mechanical properties and excellent biocompatibility in the case of binary TiNi lead to the fact that these alloys are the most widely used materials with shape memory effects and superelasticity [1,2]. Despite the almost universal use of binary TiNi for superelastic implants, these alloys

* Corresponding author: churakovaa_a@mail.ru

show insufficient fatigue during mechanocycling in the region of strain-induced martensitic transformation. Even for the first cycles, the transformation temperatures change, the superelastic deformation decreases, and residual martensite accumulates [2, 8]. Studies have shown that at 10 million cycles, the limit of fatigue endurance - the maximum amplitude of deformation - for superelastic TiNi is from 0.4 to 0.6% (whereas the "total deformation of martensite transformation" in one cycle can reach 8%) [11]. Hence, products made of TiNi, when used with a high number of cycles, can only operate in the “partial transformations” mode, which is the main disadvantage of superelastic materials based on TiNi [5–7]. SPD and subsequent annealing can be used to obtain ultrafine-grained (UFG) and nanocrystalline (NC) samples of alloys of the TiNi system of much larger size [3, 4, 12]. Several studies show that alloys based on TiNi in UFG and NC state show increased stability [8,9,13]. Active studies on the application of severe plastic deformation methods on TiNi alloys have shown interesting results: equal-channel angular pressing (ECAP) leads to structure refinement down to 300 nm [7–27], such an ultrafine-grained structure contributes to good thermal cyclic stability and a high level of mechanical properties [24-26]. The results of studies of the corrosion characteristics of titanium nickelide are contradictory. Some consider titanium nickelide to be both easy to corrode and resistant to it, comparing its anticorrosion properties with pure titanium [27-29]. The work [27] describes the electrochemical behavior and corrosion resistance of titanium nickelide. In this work, the composition, thickness, structure, and electrical properties of anode films are studied depending on the time of their formation in the active medium. The dependences obtained made it possible to describe the process of anodic dissolution of titanium nickelide within the model of selective dissolution of one of the alloy components with simultaneous oxidation of the second component. The study of the distribution profiles of elements over the depth of the anode film showed that the concentration gradient of titanium and nickel ions is directed towards the surface, and the concentration gradient for oxygen is in the opposite direction. Potentiodynamic measurements carried out showed that both components of titanium nickelide alloys are passivated in sulfuric acid. Polarization curves, which were taken in river water of the composition (mg/l: $NaHCO_3$ - 300, $CaCl_2$ - 50, $MgSO_4$ - 50) indicate that only a weak and short-term release of oxygen is possible on pure titanium at a potential of 1.6 V [27], then it is suppressed in parallel with the ongoing anodic oxidation of titanium, leading to a thickening of the oxide film. On the contrary, nickel, due to the presence of chlorides in river water, is difficult to passivate and, at a potential of 0.4-0.5 V, is subjected to pitting corrosion. Nickel contributes to a significant extent to the increase in the electronic conductivity of the films formed on its alloys with titanium. The protection of titanium nickelide from corrosion, especially local corrosion, is due to the presence of an outer layer of a film of titanium oxides on its surface, the denser and more uniform in structure and phase composition the oxide layer, the higher the corrosion resistance of titanium nickelide and the closer it approaches titanium in terms of corrosion properties and alloys based on it [27]. It has been established by electron diffraction analysis that titanium and nickel oxides in the anode film exist in the form of separate phases, and not in the form of a complex titanium oxide - nickel. It was found that the structure of titanium oxide at low potentials is close to anatase, and at high potentials it is close to rutile. There are no systematic studies on the corrosion of TiNi alloys with different structures in the literature; similarities and differences in the corrosion properties of titanium nickelide in the austenitic and martensitic states with different microstructures have not been revealed. Thus, there are no studies on the effect of deformation-thermal effects on the corrosion and electrochemical properties of titanium nickelide with different microstructures in the martensitic and austenitic states. There are no recommendations for improving the corrosion resistance of titanium nickelide.

There are no systematic studies on the corrosion of titanium nickelide with UFG structure in the literature; similarities and differences in the corrosion properties of titanium nickelide

in the austenitic and martensitic states with the UFG structure have not been revealed. Thus, there are practically no studies on the effect of deformation on the corrosion and electrochemical properties of nickel and titanium nickelide with an UFG structure in the martensitic and austenitic states. This article was devoted to the study of the structure of the TiNi alloy in various structural states after electrochemical corrosion tests.

## Material and methods

The study materials were a two-component alloys: $Ti_{49.0}Ni_{51.0}$ alloy, which has a B2 austenite structure at room temperature, with a bcc lattice of the CsCl type, and $Ti_{50.0}Ni_{50.0}$ alloy, that has a B19' martensite lattice at room temperature. To form a solid solution based on TiNi and to exclude the prehistory of obtaining the material, the alloy was quenched from the homogeneity region (from 800 °C) into water. After quenching, the samples were deformed by equal-channel angular pressing according to the Bc mode (6 passes) at T = 450°C. To reveal the microstructure of the initial titanium nickelide, an etchant of the following composition was used: 60% $H_2O$ + 35% $HNO_3$ + 5% HF. Structural studies of samples after corrosion tests were carried out using a scanning electron microscope (SEM) JEOL JSM-6490LV. The survey was carried out at an accelerating voltage of 20 kV using an SE detector. The parameters of electrochemical corrosion were determined using a universal potentiostat-galvanostat R-2X "Elins" in the mode of linear potential sweep at a rate of 100 mV/s in an aqueous solution of NaCl and $H_2SO_4$ in electrochemical cell with separation of the working electrode and the reference electrode by an electrolytic key. A standard ESr10101 silver chloride electrode was used as a reference electrode, and a steel bar was used as an auxiliary electrode. The study of corrosion behaviour was carried out by the gravimetric method, the samples were kept in an aqueous solution of NaCl and $H_2SO_4$ for a month. The phase composition was studied using a Rigaku Ultima IV X-ray diffractometer.

## Results

The Figure 1 shows the structure of TiNi alloy samples after contact with a corrosive medium - a solution of NaCl and $H_2SO_4$ obtained with an optical microscope. A significant degree of corrosion of the samples of $Ti_{49.0}Ni_{51.0}$ in the coarse-grained and ultrafine-grained states are observed (Figure 1, a, b). In the coarse-grained state, no significant corrosion damage is observed in the $Ti_{50.0}Ni_{50.0}$ alloy; corrosion products are clearly visible on the surface of the samples. In the ultrafine-grained state, significant corrosion damage is observed in the form of pitting, the size of which is several micrometers (Figure 1, c, d).

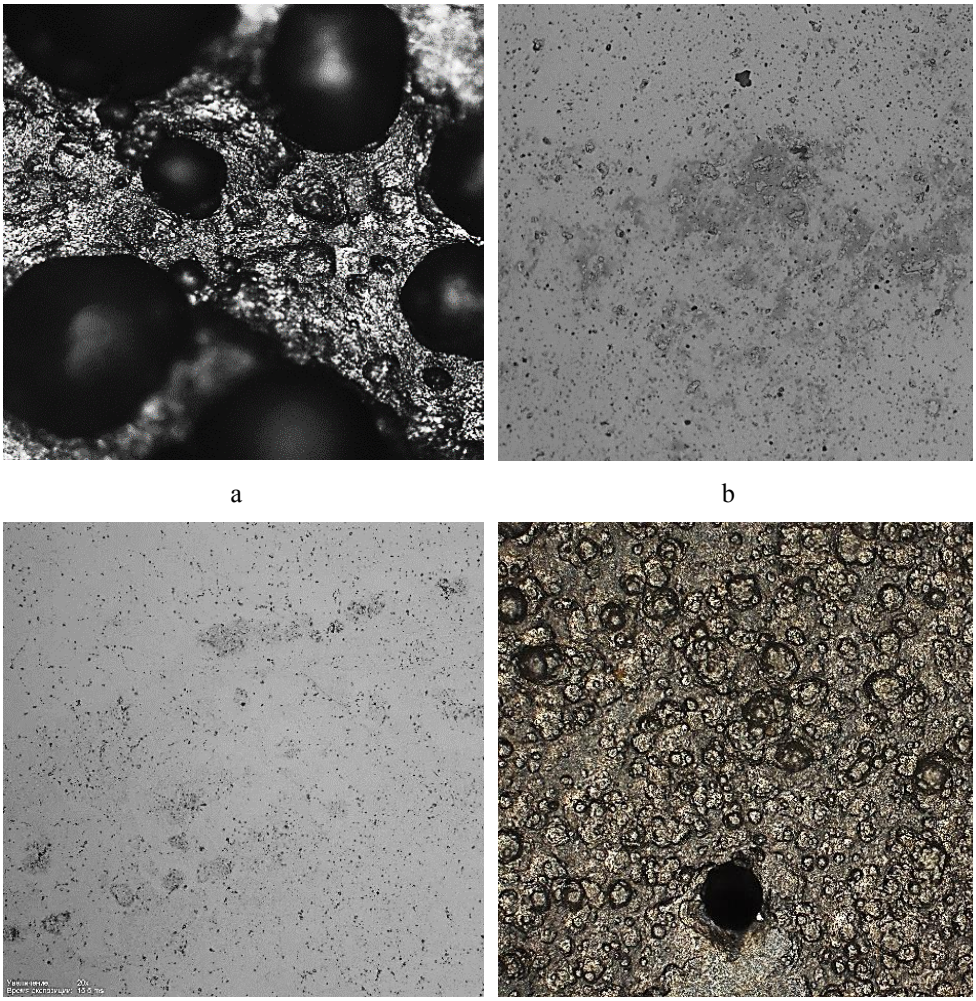

**Fig. 1.** Surface photos of $Ti_{49.0}Ni_{51.0}$ (a, b) and $Ti_{50.0}Ni_{50.0}$ alloy (c, d) samples after corrosion tests: (a, c) coarse-grained state, (b, d) ultrafine-grained state

On different parts of the surface of the sample in $Ti_{49.0}Ni_{51.0}$ alloy, there is a slight corrosion damage to the sample, which proceeds unevenly. For a more detailed study of the nature of corrosion damage, the samples were examined using an inverted microscope. On the surface of the coarse-grained alloy, deep pits are visible, which occupy more than 50% of the entire surface of the sample (Figure 2, a). Based on the images of the microstructure obtained with an inverted microscope (Figure 2, b), uniform, insignificant results of the action of an aggressive environment on the $Ti_{49.0}Ni_{51.0}$ alloy are observed on the surface of the sample. When an ultrafine-grained alloy interacts with an aggressive medium, the corrosion process proceeds without significant damage to the sample.

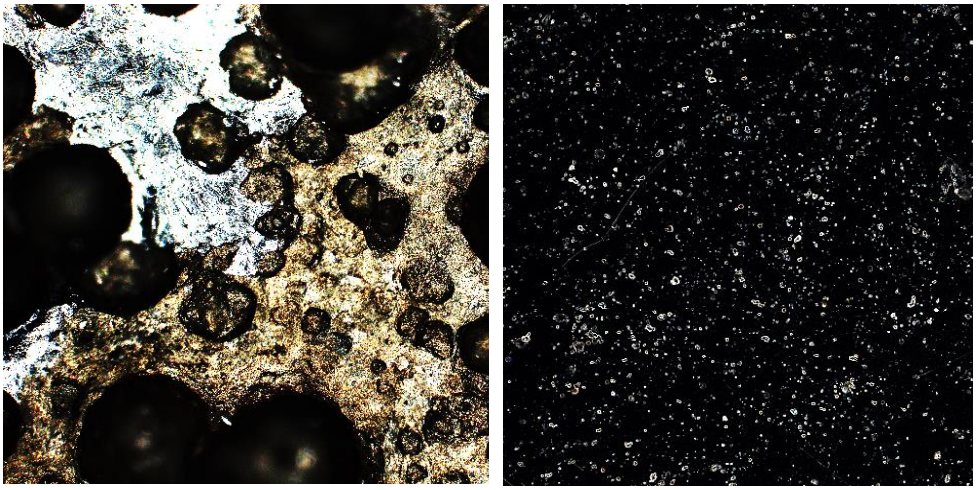

a b

**Fig. 2.** Surface photos of $Ti_{49.0}Ni_{51.0}$ samples after corrosion tests: (a) coarse-grained state, (b) ultrafine-grained state. The study was performed on an inverted microscope

In the course of the gravimetric studies, it was found that the $Ti_{49.0}Ni_{51.0}$ alloy in the coarse-grained and ultrafine-grained states has a different rate of corrosion destruction. So, for a CG alloy, the mean corrosion rate is $V_{av} = 4.46$ g/m$^2$*h, while for a UFG sample $V_{av} = 0.039$ g/m$^2$*h. Thus, the rate of the corrosion process for the coarse-grained $Ti_{49.0}Ni_{51.0}$ alloy is almost 114 times higher than for the ultrafine-grained state. The corrosion rate calculated from the gravimetric data in $Ti_{50.0}Ni_{50.0}$ alloy is $V_{av} = 0.015$ g/m$^2$*h for a CG state and $V_{av} = 5.41$ g/m$^2$*h for UFG state. Thus, the corrosion rate in the ultrafine-grained state is much higher than in the coarse-grained state, which can be explained by the higher density of defects and the phase component. However, corrosion indicators can be somewhat overestimated, which requires additional studies.

To analyze such significant differences in the corrosion behavior of TiNi alloys with different microstructures, X-ray phase analysis was carried out. The study revealed the presence of a coarse fraction of $TiNiH_{1.4}$ hydride, after corrosion tests, in a coarse-grained state in the $Ti_{49.0}Ni_{51.0}$ alloy. In the ultrafine-grained state, only the TiNi phase is observed. The data of X-ray phase analysis of the $Ti_{49.0}Ni_{51.0}$ alloy after corrosion tests in CG and UFG states are presented in the form of an X-ray diffraction pattern (Figure 3, a). Similar studies on the $Ti_{50.0}Ni_{50.0}$ alloy showed that a high proportion of the $TiNiH_{1,4}$ phase is observed in the ultrafine-grained state, compared with the volume fraction of this phase in the coarse-grained state (Figure 3, b).

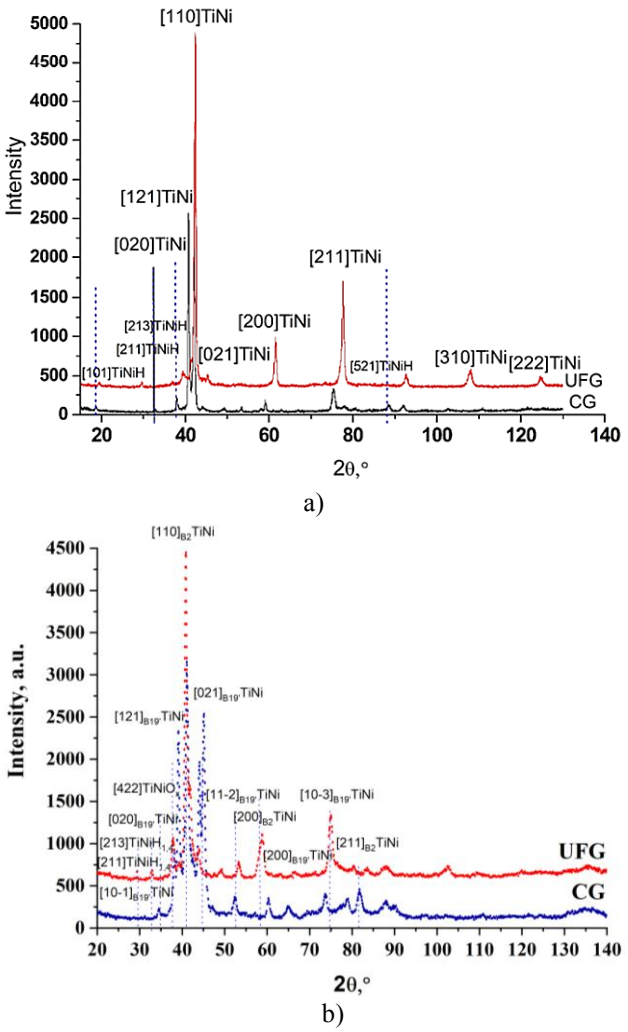


**Fig. 3.** X-ray diffraction patterns of $Ti_{49.0}Ni_{51.0}$ (a) and $Ti_{50.0}Ni_{50.0}$ (b) alloys samples after corrosion tests

According to the data obtained using X-ray phase analysis, in the initial state, before the corrosion tests, in the coarse-grained and ultrafine-grained state, the TiNi alloy was austenite to a large extent, and a small part of martensite and a $Ti_2Ni$ phase is also observed. After corrosion tests in the coarse-grained state, 3 phases are observed: austenitic, martensitic and R-phase. In the ultrafine-grained state, 3 phases are also observed, all of which correspond to the TiNi matrix, the volume fraction of the austenite phase increased with a slight decrease in the B19' martensite phase and the formation of R-martensite. The formation of the TiNi hydride - $TiNiH_{1.4}$ is probably associated with a large proportion of the Ti2Ni phase in the initial coarse-grained state, which is most prone to the formation of TiNi hydrides. While the lower content of this phase in the ultrafine-grained state promotes the formation of R - martensite and corrosion products in the main time. Also, in a coarse-grained sample before corrosion studies, austenite is 80.8%, while in the ultrafine-grained state, the volume fraction of austenite is 89.2%. As is known, an alloy in the austenitic state is more corrosion resistant, since it has a smaller number of defects compared to the martensitic state. Analyzing in aggregate the obtained data on the influence of the structural state of the alloy and the grain

size, it can be assumed that the austenitic structure is covered with passivating films for TiNi in the UFG state.

Formation of the hydride of TiNi due to the higher proportion of the $Ti_2Ni$ phase in the initial ultrafine-grained state compared to the coarse-grained state. This is probably related to the fact that corrosion in the ultrafine-grained state proceeds more actively and with the formation of pits. In addition, 5.3% of the $Ti_3Ni_3O$ phase is observed in the ultrafine-grained state, while this phase was not found in the coarse-grained state. There is also a redistribution of the phase of the TiNi matrix in the ultrafine-grained state with a larger proportion of the martensite phase.

Figure 4 shows the polarization curves of TiNi alloys taken in an aqueous solution of NaCl and $H_2SO_4$ in the coarse-grained and ultrafine-grained states.

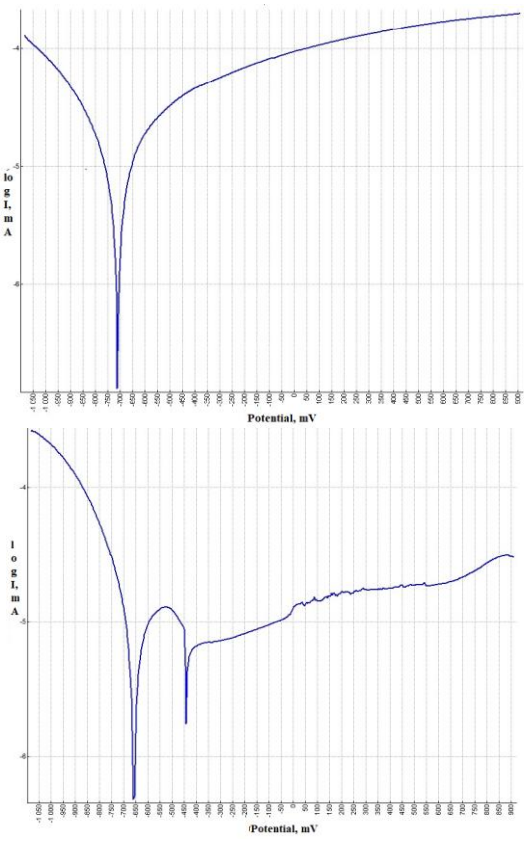


a b

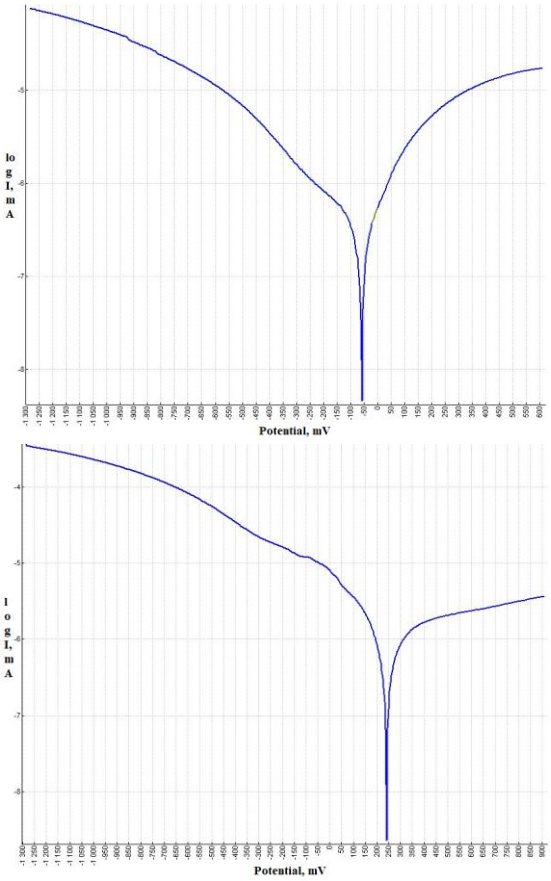


c d

**Fig. 4.** Polarization curves of $Ti_{50.0}Ni_{50.0}$ (a, b) and $Ti_{49.0}Ni_{51.0}$ (c, d) alloys and in NaCl and $H_2SO_4$ solution in coarse-grained (a, c) and ultrafine-grained (b, d) states

## Conclusions

In the coarse-grained $Ti_{50.0}Ni_{50.0}$ alloy, no significant corrosion damage is observed; corrosion products are clearly visible in a dark field taken with an inverted microscope. In the ultrafine-grained state, significant corrosion damage is observed in the form of pitting, the size of which is several micrometers. Studies of the $Ti_{49.0}Ni_{51.0}$ alloy in the coarse-grained and ultrafine-grained states showed that the rate of corrosion failure in the coarse-grained alloy is more than 114 times higher than in the ultrafine-grained one. In the photographs of the surface of the microstructure of a coarse-grained sample, corrosion destruction is observed - deep lesions of different diameters and depths, which are located over the entire surface of the alloy. In the images of the microstructure of the ultrafine grained alloy, minor effects can be seen after the corrosion tests carried out, which did not affect the integrity of the sample. X-ray phase analysis of TiNi alloys revealed that as a result of corrosion processes, the phase composition of the alloy changes, accompanied by the formation of TiNi hydride - $TiNiH_{1.4}$. In the ultrafine-grained state, the volume fraction of the formed hydride is higher than in the coarse-grained state. This is typical for both alloys, however, in the martensitic alloy, the

volume fraction is higher than in the austenitic one. Also, in the coarse-grained sample in the alloy before corrosion studies, austenite is 80.8%, while in the ultrafine-grained state, the volume fraction of austenite is 89.16%. As is known, an alloy in the austenitic state is more corrosion resistant, since it has a smaller number of defects compared to the martensitic state. Analyzing in aggregate the obtained data on the influence of the structural state of the alloy and the grain size, it can be assumed that the austenitic structure is covered with passivating films for the TiNi alloy in the UFG state. Conducted tests by the method of electrochemical corrosion showed a similar trend in behavior in a corrosive environment.

This work was supported by the Council for Grants of the President of the Russian Federation for State Support of Young Russian Scientists - Candidates of Science (MK-6202.2021.1.2). Kayumova E.M. is grateful was supported within the framework of work on the state task Ministry of Education and Science of the Russian Federation for FGBOU VO "UGATU" (agreement No. 075-03-2021-014/4) in youth research laboratory "Metals and Alloys under Extreme Impacts".

## References

1. Khachin V.N., Pushin V.G., Kondratiev V.V. Titanium nickelide, structure and properties, Nauka, 1992, 161 p.

2. Shape Memory Alloys: Fundamentals, Modeling and Applications. /Ed. by: V. Brailovski, S. Prokoshkin, P. Terriault and F. Trochu, Montreal, Ecole de technologie superieure (ETS), Universite du Quebec, Canada, 2003, 851 p.

3. Valiev R.Z., Zhilyaev A.P., Langdon T.G. Bulk Nanostructured Materials: Fundamentals and Applications, 2014, John Wiley & Sons, Inc., Hoboken, New Jersey, 456 p.

4. R.Z. Valiev, I.V. Aleksandrov, Bulk nanostructured metallic materials: preparation, structure and properties, Akademkniga, 2007, 398 p.

5. V.G. Pushin, V.V. Stolyarov, D.V. Gunderov, R.Z. Valiev, T.C. Lowe, Y.T. Zhu Nanostructured TiNi-based shape memory alloys processed by severe plastic deformation // Mater. Sci and Eng. A, 2005.

6. D. Gunderov, A. Lukyanov, E. Prokofiev, V. Pushin Mechanical properties of the nanocrystalline Ti49.4Ni50.6 alloy, produced by high pressure torsion Eur. Phys. J., 158, 53-58 (2008).

7. V.V. Stolyarov, E.A. Prokofiev, S.D. Prokoshkin, S.V. Dobatkin, I.B. Trubitsyna, I.Yu. Khmelevskaya, V.G. Pushin, R.Z. Valiev Structural features, mechanical properties and the shape memory effect in TiNi alloys obtained by equal-channel angular pressing, Physics of metals and metallurgy, 2005. V. 100. No. 6. S. 91.

8. Churakova A.A., Gunderov D.V. Transformation of the TiNi Alloy microstructure and the Mechanical Properties Caused by Repeated B2-B19′ Martensitic Transformations // Acta Metallurgica Sinica (English Letters): V. 28, Issue 10, 2015, P. 1230-1237

9. Y.X. Tong, B. Guo, F. Chen, B. Tian, L. Li, Y.F. Zheng, Egor A. Prokofiev, Dmitry V. Gunderov Ruslan Z. Valiev Thermal cycling stability of ultrafine-grained TiNi shape memory alloys processed by equal channel angular pressing Scripta Materialia 67 (2012) pp. 1–4.

10. Yintao Song, Xian Chen, Vivekanand Dabade, Thomas W. Shield & Richard D. James Enhanced reversibility and unusual microstructure of a phase-transforming material Nature 2013, V.502, P. 85

11. Christoph Chluba, Wenwei Ge, Rodrigo Lima de Miranda, Julian Strobel, Lorenz Kienle, Eckhard Quandt, Manfred Wuttig Ultralow-fatigue shape memory alloy films Science, 2015 V.348, Is. 6238

12. Valiev R.Z., Pushin V.G., Gunderov D.V., Popov A.G. The use of severe deformations to obtain bulk nanocrystalline materials from amorphous alloys // Dokl. RAN. 2004. V. 398. No. 1. S. 54-56.

13. Yunxiang Tong and Yong Liu, Effect of precipitation on two-way shape memory effect of melt-spun Ti50Ni25Cu25 ribbon, Materials Chemistry and Physics 120 (2010) 221–224

14. Gunderov D.V., Pushin V.G., Valiev R.Z., Valiev E.Z. Structural and phase transformations in an amorphous rapidly quenched Ti–Ni–Cu alloy subjected to severe plastic deformation and heat treatment // Deformation and destruction of materials. 2006. No. 4. S. 22-25.

15. Zhao L.C., Duerig T.W., Justi S., Melton K.N., Proft J.L., Yu W, et al. The study of niobium-rich precipitations in a NiTiNb shape memory alloy. Scr Met Mater 1990; 24:221-225.

16. Zhang C.S., Zhao L.C., Duerig T.W., Wayman C.M. Effects of deformation on the transformation hysteresis and shape memory effect in a Ni47Ti44Nb9 alloy. Scr Met Mater 1990; 24:1807-1812.

17. Zhang C.S., Wang Y.Q., Cai W., Zhao L.C. The study of constitutional phases in a Ni47Ti44Nb9 shape memory alloy. Mater Chem Phys 1991; 28:43-50.

18. Piao M., Miyazaki S., Otsuka K. Characteristics of deformation and transformation in Ti44Ni47Nb9 shape memory alloy. Mater Trans JIM 1992; 33:346-353.

19. Sui J.H., Gao Z.Y., Li Y.F., Zhang Z.G., Cai W. A study on NiTiNbCo shape memory alloy. Mater Sci Eng A 2009; 508:33-36.

20. Chen Y., Jiang H.C., Rong L.J., Xiao L., Zhao X.Q. Mechanical behavior in NiTiNb shape memory alloys with low Nb content. Intermetallics 2011; 19:217-220.

21. Pushin V.G., Stolyarov V.V., Valiev R.Z., Kourov N.I., Kuranova N.N., Prokofiev E.A., et al. Features of structure and phase transformations in shape memory TiNi-based alloys after severe plastic deformation. Ann Chim Sci Mat 2002; 27:77-88.

22. Pushin V.G., Stolyarov V.V., Valiev R.Z., Lowe T.C., Zhu Y.T. Nanostructured TiNibased shape memory alloys processed by severe plastic deformation. Mater Sci Eng A 2005;410-411:386-389.

23. Prokoshkin S.D., Khmelevskaya I.Yu., Dobatkin S.V., Trubitsyna I.B., Tatyanin E.V., Stolyarov V.V. et al. Alloy composition, deformation temperature, pressure and post-deformation annealing effects in severely deformed TieNi based shape memory alloys. Acta Mater 2005; 53:27032714.

24. Kockar B., Karaman I., Kim J.I., Chumlyakov Y. A method to enhance cyclic reversibility of NiTiHf high temperature shape memory alloys. Scr Mater 2006; 54:2203-2208.

25. Kockar B., Karaman I., Kim J.I., Chumlyakov Y.I., Sharp J, Yu CJ. Thermomechanical cyclic response of an ultrafine-grained NiTi shape memory alloy. Acta Mater 2008; 56:3630-3646.

26. Tong Y.X., Guo B., Chen F., Tian B., Li L., Zheng Y.F. et al. Thermal cycling stability of ultrafine-grained TiNi shape memory alloys processed by equal channel angular pressing. Scr Mater 2012; 67:1-4.

27. T.N. Ustinskaya, N.D. Tomashov, E.N. Lubnik, Composition, electrochemical and protective properties of anode films based on TiNi intermetallide, Electrochemistry 23(1987) 254-259.

28. Tan, L. Corrosion and wear – corrosion behavior of NiTi modified by plasma source ion implantation/ R. A. Dodd, W.C. Crone// Biomaterials. -2003 (24)-p. 3931-3939.

29. Okazaki, Y. Corrosion resistance, mechanical properties, corrosion fatigue strength and cytocompatibility of new Ti alloys without Aland V/Y. Okazaki, S. Rao, Y. Yto // Biomaterials. - 1998 (19), p. 1197-1215.